Radio Science, Volume ???, Number , Pages 1–22,

Sensitivity of microwave brightness temperatures to hydrometeors in tropical deep convective cloud system at 89–190 GHz

Gang Hong and Georg Heygster

Institute of Environmental Physics, University of Bremen, Bremen, Germany

Jungang Miao

Electromagnetics Laboratory, Baihang University, Beijing, China

Klaus Kunzi

Institute of Environmental Physics, University of Bremen, Bremen, Germany

Submitted to Radio Science, July 2004.

Gang Hong, Georg Heygster, and Klaus Kunzi, Institute of Environmental Physics, University of Bremen, Post Box 330440, Bremen 28334, Germany. (honggang@uni-bremen.de)

Jungang Miao, Electromagnetics Laboratory, Baihang University, Beijing 100083, China.

The sensitivity of microwave brightness temperatures at the frequencies between 89 and 190 GHz to surface emissivities and hydrometeors in a deep convective cloud system is investigated by simulations, using the Goddard Cumulus Ensemble (GCE) model data of a simulated oceanic tropical squall line as input for a radiative transfer model. It is found that only the window channel at 89 GHz has an apparent dependence on the surface emissivity. The three water vapor channels around 183 GHz (i.e., 183.3 $\pm$ 1, $\pm$3, and $\pm$7 GHz) are completely independent and the window channel at 150 GHz is nearly independent on the surface emissivity due to the atmospheric opacity at these frequencies. All channels are apparently influenced by deep convective clouds and their outflowing thick cirrus clouds. The channels at 89, 150, and 183.3 $\pm$ 7 GHz are strongly sensitive to variations in the liquid water content at levels above 5 km. The sensitivity of the channel at 150 GHz to liquid water is about twice the ones at 89 and 183.3$\pm$7 GHz. All channels are generally sensitive to variations in the frozen hydrometeor content at levels above 7 km. The 183.3 $\pm$ 1 GHz channel has virtually no influence from the frozen hydrometeors at levels below 7 km. The sensitivity suggests that it should be possible to estimate the frozen hydrometeor properties in levels above 7 km in tropical deep convective clouds using the water vapor channels around 183 GHz.

1. Introduction

Microwave radiometric measurements of precipitation systems have been conducted from both aircraft and satellite platforms for two decades [e.g., *Wilheit et al.*, 1982; *Adler et al.*, 1990; *Vivekanandan et al.*, 1991]. Most of them make use of radiometric signatures at frequencies below 90 GHz, such as the Special Sensor Microwave/Image (SSM/I) and the Tropical Rainfall measuring Mission Microwave Imager (TRMM TMI). Frequencies between 85 and 190 GHz are exploited by the Special Sensor Microwave Temperature 2 (SSM/T2) onboard DMSP satellites, by the Advanced Microwave Sounding Unit (AMSU)-B onboard NOAA-15, 16, and 17, and by the AMSU/HSB (Humidity Sounder for Brazil) onboard Aqua. The key advantage of frequencies between 85 and 190 GHz is the unique ability to penetrate most clouds [e.g., *Burns et al.*, 1997; *Greenwald and Christoper*, 2002]. However, the atmosphere is not entirely transparent at these frequencies in cases where thick clouds or precipitation significantly contaminate the sounder's field of view [*Eyre*, 1990]. Consequently, the effects of cloud and precipitation provide possibilities to estimate cloud parameters, especially at the frequencies around 89 and 150 GHz [e.g., *Liu and Curry*, 1999; *Zhao and Weng*, 2002; *Weng et al.*, 2003].

The effects of clouds and precipitation on microwave radiances at the AMSU-B channels have been examined through simulations [e.g., *Muller et al.*, 1994; *Burns et al.*, 1997; *Skofronick-Jackson et al.*, 2002; *Bennartz and Bauer*, 2003] and observations [e.g., *Wang et al.*, 1997, 1998; *Greenwald and Christoper*, 2002]. The hydrometeors in the upper altitude levels of clouds with high cloud top results in

large brightness temperature depressions at the AMSU-B frequencies of 150 GHz and above. Furthermore, for the three channels around the water vapor absorption line centered at 183.3 GHz (i.e., 183.3 ± 1, ± 3, ± 7 GHz), the farther the frequency is from the center, the larger is the brightness temperature depression [*Burns et al.*, 1997]. This is because the more distant channels can view deeper into clouds than the other ones do. The temperature weighting functions of the three water vapor channels reach their maxima at different altitudes for precipitating clouds [*Burns et al.*, 1997], suggesting a potential to delineate the distribution of hydrometeors in clouds [*Wang et al.*, 1997, 1998; *Skofronick-Jackson and Wang*, 2000].

In typical midlatitude atmospheres, *Muller et al.* [1994] studied the influence of surface emissivities, water vapor, cloud liquid water, and ice particles in nonprecipitating clouds on brightness temperatures at AMSU-B like frequencies. They documented that the brightness temperature at 89 GHz is stronger affected by altostratus liquid clouds than by cirrus clouds for equivalent water paths. Brightness temperatures at frequencies above 150 GHz are stronger affected by ice clouds. For precipitating clouds, the information content of observations at the AMSU-B frequencies depends crucially on the particle size distribution, particle density, mixing rule, and cloud height [*Gasiewski*, 1992; *Burns et al.*, 1997; *Skofronick-Jackson and Wang*, 2000; *Bennartz and Petty*, 2001; *Skofronick-Jackson et al.*, 2002; *Bennartz and Bauer*, 2003]. Also *Bennartz and Bauer* [2003] investigated the sensitivity of microwave radiances at the frequencies from 85 to 183 GHz to ice particle scattering and to various environmental parameters (i.e., water vapor and surface emissivity) at middel and

high latitude conditions. They found under these conditions with cloud tops below 8 km and little water vapor burden that the water vapor channels closer the water vapor absorption line at 183.3 GHz (i.e., 183.3 ± 3 and 183.3 ± 1 GHz) show a weak or negligible response to precipitating clouds because their weighting functions peak too high up in the atmosphere [*Bennartz and Bauer*, 2003; *Kim et al.*, 2003].

However, in the tropics the situation is very different: The water vapor burden increases from annual mean values of 2.5 $\mathrm{kg\,m^{-2}}$ in polar regions to over 50 $\mathrm{kg\,m^{-2}}$ in the tropics [*Peixoto and Oort*, 1992] so that the sensitivity to the surface is much lower and the maxima of the weighting functions of the water vapor channels are shifted to higher altitudes [*Burns et al.*, 1997; *Staelin and Chen*, 2000]. On the other hand, the deep convective clouds extend over 10 km in height and even can penetrate into the the tropical tropopause layer at 14–18 km [e.g., *Alcala and Dessler*, 2002].

These differences to the well investigated middle and high latitude conditions are so fundamental that it appears worth to dedicate a microwave sensitivity study to hydrometeors in tropical deep convective clouds. In this study, the sensitivity of the microwave brightness temperatures at the AMSU-B channels to the hydrometeors in deep clouds related to an oceanic tropical squall line system, as well as to the surface emissivity, are investigated using the simulated microphysical data obtained from the Goddard Cumulus Ensemble (GCE) model. In Section 2, the cloud model data and a microwave radiative transfer model are introduced. In order to investigate the sensitivity for different clouds generated in the squall line, the cloud model data are classified into four types: thin cirrus cloud, thick cirrus cloud, deep convective

cloud, and other clouds. In Section 3, the sensitivity of brightness temperatures to the surface emissivity is investigated for the different cloud types. In Section 4, with hydrometeor data from one vertical cross section of the simulated squall line, the sensitivity of the brightness temperatures to variations in the hydrometeor water contents is investigated. Our results are summarized in Section 5.

2. Cloud Model Data and Radiative Transfer Model

Using nearby composite aircraft and radiosonde sounding data as initial environmental field, an oceanic tropical squall line was simulated by a realistic dynamical cloud model, the Goddard Cumulus Ensemble (GCE) model developed by *Tao and Simpson* [1993]. The model domain is a $128 \times 128 \times 31$ grid with a horizontal resolution of 1.5 km and a vertical resolution increasing from 0.2 to 1.0 km from bottom to top at about 20 km. The GCE cloud model distinguishes five types of hydrometeors, namely cloud liquid water, rain water, cloud ice, snow, and graupel. Profiles of temperature and water vapor are also obtained along with profiles of the hydrometeors. The GCE data at the model times of 240 and 360 minutes are used for simulations in this study. Because our study is focussed on deep convective system, only clouds with a top above 8 km are considered. The clouds are classified into four types, thin cirrus, thick cirrus, deep convective, and other clouds, mainly comprising shallow precipitating and stratiform clouds. The classification results are shown in Figure 1. The cross section of hydrometeor water contents of liquid water (cloud water plus

rain water), cloud ice, snow, and graupel along $x = 58$ indicated by the solid black line in Figure 1 are shown in Figure 2.

The discrimination of cirrus clouds is based on the method of *Mace et al.* [2001] and *Luo et al.* [2003]. According to their method, to qualify a cloud layer as cirrus, the temperature at the cloud top must be less than $-35°$C and the temperature at the altitude level of maximum total ice water content must be less than $-20°$C. This method ensures that ice microphysical processes are dominant in the generation region near the cloud top, but excludes deep convective cloud layers that are capped by ice-phase clouds [*Luo et al.*, 2003]. Furthermore, thin cirrus cloud is defined as cirrus cloud with low total ice water path ($\leq$0.5 kg m^{-2}), and thick cirrus cloud is defined as cirrus cloud exceeding this threshold. Deep convective clouds normally have a large frozen hydrometeor water content in the upper layers [e.g., *Cifelli et al.*, 2002; *Skofronick-Jackson et al.*, 2003]. The radar reflectivities of the deep convective clouds at the altitude of 10 km are around 20 dBZ [e.g., *Cifelli et al.*, 2002; *Geerts et al.*, 2000; *Kelley and Stout*, 2004]. Using the empirical relationship of *Heymsfield and Palmer* [1986] between radar reflectivity and cloud ice water content, 20 dBZ radar reflectivity corresponds to about 0.52 g m^{-3} cloud ice water content. Therefore, the GCE cloud model data with cloud top height above 10 km and the layers above 10 km having total ice water content values above 0.5 g m^{-3} are classified as deep convective clouds. The remaining components are classified as other clouds. The averaged total ice water paths of thin cirrus, thick cirrus, deep convective, and other

clouds are 0.08, 0.66, 7.38, and 1.27 $\mathrm{kg\,m^{-2}}$, respectively. The averaged water vapor is about 60 $\mathrm{kg\,m^{-2}}$ for each cloud type.

A microwave radiative transfer model (RTM) without employing a melting layer [*Kummerow et al.*, 1996] is used to calculate the microwave upwelling brightness temperatures between 89 and 190 GHz. It considers the same five hydrometeor types as those obtained from the GCE cloud model data. All hydrometeors are treated as Mie spheres. The Maxwell-Garnett mixing theory [*Bohren and Battan*, 1980] is used in the RTM for the ice and air mixtures of frozen hydrometeors to obtain the dielectric constant. The size distributions of rain, snow, and graupel are assumed to be exponentially distributed with

$$N(D) = N_0 \exp(-\lambda D), \tag{1}$$

where D is the diameter of particles, N_0 is the intercept parameter, and λ is the slope of the distribution depending on N_0, the density of hydrometeor, and the hydrometeor water content. N_0 values used in this study are 2.2×10^7 $\mathrm{m^{-4}}$ for rain, 10^8 $\mathrm{m^{-4}}$ for snow, and 4×10^6 $\mathrm{m^{-4}}$ for graupel. The same N_0 values have been used in the TRMM version 6 of the 2A12 algorithm to retrieve hydrometeor profiles (Haiyan Jiang, personal communication). The densities of rain, snow, and graupel are 1.0, 0.1, and 0.6 $\mathrm{g\,m^{-3}}$, respectively [*Burns et al.*, 1997]. *Wang et al.* [1997, 1998] suggested that cloud ice in the upper portion of convection should be taken into account for radiative transfer calculations at high frequencies of the AMSU-B channels. The distribution of cloud ice included in this version of the RTM is the one given by the fit to observed cloud ice distributions by *Heymsfield and Platt* [1984]. The particle

size of cloud water is a gamma distribution as shown by *Liou* [1992]. The densities of cloud ice and cloud liquid water are respectively 0.917 and 1.0 $\mathrm{g\,m^{-3}}$.

3. Brightness Temperature Depressions and Sensitivity to Surface Emissivities

The brightness temperatures at the frequencies between 89 and 190 GHz simulated by the GCE data are averaged over each of the four cloud types, respectively, under different surface emissivities varying from 0.5 to 1.0 with intervals of 0.05. The background brightness temperatures at these frequencies are also simulated by the GCE data, but without cloud hydrometeors. The brightness temperature depressions, i.e., the differences between the background brightness temperatures and the brightness temperatures over clouds are shown in Figure 3.

When the atmosphere becomes optically thicker (e.g., from cirrus cloud to deep convective cloud), the brightness temperature depressions increase. They are below 1 K for all channels over thin cirrus clouds, but they are much larger for deep convective clouds, especially at the channels away from the water vapor absorption line centered at 183.3 GHz. For all channels the brightness temperature depressions vary strongly with the cloud type.

For all cloud types, the water vapor channels farther away from the water vapor absorption center have larger brightness temperature depressions as these channels can see deeper into the cloud, hence being subjected to greater scattering from the lower layers [*Burns et al.*, 1997; *Wang et al.*, 1997]. For thin cirrus clouds, the 183.3$\pm$ 7 GHz channel has a larger brightness temperature depression than the 150 GHz

channel. However, the situation for thick cirrus, deep convective, and other clouds is inverse. The brightness temperature depression at 150 GHz is about 1.5 times larger than that at 183.3 ± 7 GHz for deep convective clouds and 2.4 times for other clouds. This is similar to the result of *Bennartz and Bauer* [2003] that the observed scattering signal at 150 GHz is about twice that at the 183.3 ± 7 GHz for all their investigated cases. The reason is the increased impact of water vapor in and above the clouds that tends to mask the scattering signal in the water vapor channels. For thick cirrus and deep convective clouds, even the 183.3 ± 1 GHz channel still has some influence from clouds, and its brightness temperature depressions are about 1.7 and 6.5 K, respectively. The effects of clouds on 183.3 ± 1 GHz in our cases are different from the results of *Bennartz and Bauer* [2003] which indicate that the precipitation events can not be detected at all at 183.3 ± 1 GHz. The difference is caused by the cloud structure. The intensive thunderstorm case investigated by *Bennartz and Bauer* [2003] has a maximum vertical extent of about 10 km. However, the deep convective clouds and thick cirrus clouds investigated in our study still have large frozen hydrometeors above 10 km and extend up to 14 km altitude so that the 183.3 ± 1 GHz channel still shows a measurable effects from the upper frozen hydrometeors.

Only the 89 GHz channel has an apparent dependence on surface emissivity, and the 150 GHz channel shows a very small dependence. The three water vapor channels around 183.3 GHz are practically insensitive to the surface emissivity (Figure 3). The impacts of uncertainties and variations in the surface emissivity on the differ-

ent channels are also investigated using the method of *Bennartz and Bauer* [2003]. The changes in brightness temperatures resulting from an increment in the surface emissivity by 0.1 are calculated at the different channels for the four types of clouds. For all cloud types, the 89 GHz channel shows the strongest influence. The changes in brightness temperatures for thin cirrus, thick cirrus, deep convective, and other clouds are about 50, 46, 4, and 23 K , respectively. The 89 GHz channel exhibits the strongest responses for a more transparent atmosphere (e.g., thin cirrus clouds and thick cirrus clouds). However, the 150 GHz channel only has weak influence of about 2 K for thin cirrus and thick cirrus clouds. The three water vapor channels show no influence from the variations of the surface emissivity. This is due to the opaque atmosphere at these channels [*Greenwald and Christoper*, 2002; *Bennartz and Bauer*, 2003].

4. Sensitivity to Hydrometeor Water Contents in Deep Convective Cloud

The brightness temperature Jacobians with respect to hydrometeors in deep convective cloud are calculated to investigate the sensitivity of the brightness temperatures to variations in the hydrometeor water contents. For one layer of hydrometeor, the Jaccobian in $\mathrm{K\,m^3\,g^{-1}}$ is expressed as $\Delta T_b/\Delta w$, where Δw is a 5% increase in hydrometeor water content in $\mathrm{g\,m^{-3}}$, and ΔT_b is the brightness temperature change in K caused by this variation. The vertical distribution of the Jacobians is obtained by calculating it separately for all layers of hydrometeors. Since the GCE model data are simulated for an oceanic squall line, the surface emissivities at all considered fre-

quencies are set to a typical value of 0.7 [*Muller et al.*, 1994]. The simulations at nadir along the vertical cross section at $x = 58$ in Figure 2 are used to investigate the sensitivity.

Figure 4 shows the brightness temperature Jacobians with respect to liquid water content (cloud liquid water plus rain water) for all channels. Those at 89, 150, and 183.3 ± 7 GHz are very sensitive to variations in liquid water content at high altitudes from 5 to 10 km. The 150 GHz channel is most sensitive to liquid water. The increase in brightness temperature at 150 GHz resulting from the increase in liquid water content is higher than that at the next sensitive frequency, 183.3 ± 7 GHz, by a factor of about 2. The increase in liquid water content generally increases the brightness temperatures at high altitudes for the 89, 150, and 183.3 ± 7 GHz channels, but in some small areas, it causes a decrease. In the channels closer to the water vapor absorption line, the regions of negative Jacobians become more and more apparent. At 183.3 ± 1 GHz, an increase in liquid water content only results in a decrease in brightness temperatures at high altitudes above 7 km. At altitudes below about 5 km, the brightness temperatures of all channels show almost no variations with the liquid water content. This indicates that the direct sensitivity to rain for all channels is very small, especailly for the water vapor channels.

Cloud ice in the upper altitudes has strong influence on the frequencies above 150 GHz [*Muller et al.*, 1994; *Wang et al.*, 1997, 1998]. The Jacobians with respect to cloud ice content are shown in Figure 5. The increase in cloud ice content results in decrease in brightness temperatures for all channels due to scattering by the ice

particles. The frequencies closer to the water vapor absorption line are more sensitive to cloud ice at higher altitudes. The window channel at 150 GHz is more than twice sensitive to cloud ice compared to the window channel at 89 GHz, and the largest sensitivity of both window channels is from similar altitudes around 8 km. The 183.3 ± 7 GHz channel has the highest sensitivity to variation in cloud ice content. The area with Jacobians less than $-25\ \mathrm{K\,m^3\,g^{-1}}$ for this channel is much larger than that for the 150 GHz channel. The Jacobians of all other channels do not exceed $-25\ \mathrm{K\,m^3\,g^{-1}}$. The 183.3 ± 1 GHz channel is apparently sensitive to higher levels above 12 km. It is not sensitive to cloud ice below 9 km because the atmosphere is opaque for this channel.

The sensitivity to snow water content is shown in Figure 6. Relative to the sensitivity to cloud ice content, the sensitivity to snow is weaker. Similar to the sensitivity to cloud ice, the channels at frequencies of 150 GHz and above are more sensitive to snow at the higher levels. However, the layers with strong sensitivity shift to higher altitude levels at about 12–13 km. Again, the 183.3 ± 7 GHz channel has the largest sensitivity to snow. Both the 183.3 ± 1 and 183.3 ± 3 GHz channels generally are insensitive to snow below 7 km. Like the sensitivity to cloud ice, because of the different penetrating ability due to the water vapor above and in the clouds and hydrometeors at high altitudes, the sensitivities to snow of the three water vapor channels becomes smaller as the channel approaches the center of the absorption line. The sensitivity to graupel (Figure 7) shows a similar behavior. The channels at frequencies above 150 GHz are most sensitive at high altitudes of about 10 to 12 km with

the 183.3 ± 7 GHz channel showing the highest Jacobian. It exceeds -70 K m^3 g^{-1}. Below 7 km the sensitivities of the three water vapor channels are negligible due to an increase in graupel water content and water vapor. The 183.3 ± 1 GHz channel generally is practically insensitive to graupel below 9 km similar to cloud ice and snow.

As disscussed in Section 3, the three water vapor channels do not show influence from surface emissions. Moreover, the sensitivity to each hydrometer type at the three water vapor channels have obvious differences (altitude levels and values). Hence, Jacobians of the brightness temperature difference between the 183.3 ± 1 GHz and the 183.3 ± 7 GHz channels (henceforth, difference Jacobians) are shown in Figure 8 for different hydrometeor types in order to investigate their potential for the retrieval of cloud parameters. In the deep convective cloud region from $y = 20$ to $y = 45$, for frozen hydrometeors the difference Jacobians are generally positive above 7 km and near to zero below 5 km. The difference Jacobians for snow are smaller than those for cloud ice and graupel, the latter having the largest values. The areas with the highest difference Jacobians for frozen hydrometeors locate at different altitudes, namely at about 9, 12, and 10.5 km for cloud ice, snow, and graupel, respectively. These different responses of the difference Jacobians in the various layers of the deep convective cloud reveal a potential to delineate the distribution of frozen hydrometeors in the upper layers of deep convective clouds, using the differences of the water vapor channels. However, liquid water contributes negatively to the brightness tem-

perature difference signal at about 9.5 km. This somewhat weakens the response of the brightness temperature differences to variations in frozen hydrometeor profiles.

5. Conclusions

The sensitivity of brightness temperatures at the AMSU-B channels to the surface emissivity and variations in the hydrometeor content in tropical deep convective cloud has been investigated by simulations with a modelled oceanic tropical squall line system. Our results partly agree with the sensitivity analyses of *Bennartz and Bauer* [2003] who used simulations of a midlatitude shallow precipitating convective cloud with cloud top height below 8 km. However, in the tropic situation with the high cloud tops (above 10 km) of deep convective systems and the much larger amount of atmospheric water vapor, the sensitivity to hydrometeor contents in tropical deep convective cloud is different from that in midlatitude shallow precipitating cloud:

1. The surface emissivity has an important influence on the brightness temperatures only at 89 GHz over deep convective systems, at 150 GHz the influence is very small. The three water vapor channels do not dependent on the surface emissivity for all clouds of tropical deep convective systems. This independence on the surface emissivity provides the advantage to obtain the isolated atmospheric influence that we observe in the three water vapor channels.

2. Thin cirrus clouds have very small influence on the brightness temperatures at the AMSU-B frequencies. The brightness temperature depressions are less than

1.0 K for all channels. However, deep convective and thick cirrus clouds have apparent influence on the brightness temperatures at these frequencies.

3. The channels at 89, 150, and 183.3 ± 7 GHz are strongly positive sensitive to variations in the liquid water content above 5 km (Figure 4). The largest sensitivity to liquid water is found at 150 GHz. It is twice that at 89 and 183.3 ± 7 GHz. Below 5 km, all channels have almost zero sensitivity to variations in the liquid water content.

4. The brightness temperature Jacobians with respect to frozen hydrometeors at all channels are generally negative due to ice scattering, only the Jacobians with respect to snow have some slightly positive values. The sensitivity to graupel at all channels is stronger than that to cloud ice and snow. The 183.3 ± 7 GHz channel shows a stronger sensitivity than the other channels do for frozen hydrometeors. At the channels closer to the water vapor absorption line, the sensitivity is strongest for frozen hydrometeors at high altitude levels. The brightness temperatures at the three water vapor channels are mainly sensitive to frozen hydrometeors above 7 km. The 183.3 ± 1 GHz channel has virtually no sensitivity to frozen hydrometeors below 7 km.

5. The brightness temperature difference between the 183.3 ± 1 GHz channel and the 183.3 ± 7 GHz channel is generally sensitive to liquid water above 5 km and frozen hydrometeors above 7 km. However, the difference Jacobians with respect to liquid water are generally negative and those with respect to frozen hydrometeors are positive. These sensitivity analyses reveal that the brightness temperatures and

brightness temperature differences at the water vapor channels of AMSU-B can be used to estimate the hydrometeor properties in the upper altitude levels of tropical deep convective clouds [*Hong*, 2004].

Acknowledgments. We thank J. Wang and G. Skofronick-Jackson for providing us with GCE cloud model data; C. Kummerow for providing and helping us with his RTM codes; H. Jiang for helping with the parameters of particle size distribution; and R. Bennartz for helpful suggestions on calculating Jacobian. G. Hong is grateful to the Gottlieb Daimler- und Karl Benz- Foundation and University of Bremen for their support.

References

Adler, R. F., R. A. Mack, N. Prasad, H.-Y. M. Yeh, and I. M. Hakkarinen (1990), Aircraft microwave observations and simulations of deep convection from 18 to 183 GHz, Part I: Observations, *J. Atmos. Ocean. Technol.*, *7*, 377–391.

Alcala, C. M., and A. E. Dessler (2002), Observations of deep convection in the tropics using the Tropical Rainfall Measuring Mission (TRMM) precipitation radar, *J. Geophys. Res.*, *107*(D24), 4792, doi:10.1029/2002JD002457.

Bennartz, R., and P. Bauer (2003), Sensitivity of microwave radiances at 85-183 GHz to precipitating ice particles, *Radio Sci.*, *38*(4), 8075, doi:10.1029/2002RS002626.

Bennartz, R., and G. W. Petty (2001), The sensitivity of microwave remote sensing observations of precipitation to ice particle size distributions, *J. Appl. Meteorol.*, *40*, 345–364.

Bohren, C. F., and L. J. Battan (1980), Radar backscattering by inhomogeneous precipitation particles, *J. Atmos. Sci.*, *37*, 1821–1827.

Burns, B. A., X. Wu, and G. R. Diak (1997), Effects of precipitation and cloud ice on brightness temperatures in AMSU moisture channels, *IEEE Trans. Geosci. Remote Sens.*, *35*, 1429–1437.

Cifelli, R., W. A. Petersen, L. D. Carey, S. A. Rutledge, and M. A. F. da Silva Dias (2002), Radar observations of the kinematic, microphysical, and precipitation characteristics of two MCSs in TRMM LBA, *J. Geophys. Res.*, *107*(D20), 8077, doi:10.1029/2000JD000264.

Eyre, J. R. (1990), The information content of data from operational satellite sounding systems: A simulation study, *Q. J. R. Meteorol. Soc.*, *116*, 401–434.

Gasiewski, A. J. (1992), Numerical sensitivity analysis of passive EHF and SMMW channels to tropospheric water vapor, clouds, and precipitation, *IEEE Trans. Geosci. Remote Sens.*, *30*, 859–870.

Geerts, B., G. M. Heymsfield, L. Tian, J. B. Halverson, A. Guillory, and M. I. Mejia (2000), Hurricane Georges's landfall in the Dominican Republic: Detailed airborne doppler radar imagery, *Bull. Amer. Meteorol. Soc.*, *81*, 999–1018.

Greenwald, T. J., and S. A. Christoper (2002), Effect of cold clouds on satellite measurements near 183 GHz, *J. Geophys. Res.*, *107*(D13), 4170, doi: 10.1029/2000JD000258.

Heymsfield, A. J., and A. G. Palmer (1986), Relationships for deriving thunderstorm anvil ice mass for CCOPE storm water budget estimates, *J. Clim. Appl. Meteor*, *25*, 691–702.

Heymsfield, A. J., and C. M. R. Platt (1984), A parameterization of the particle size spectrum of ice clouds in terms of the ambient temperature and the ice water content, *J. Atmos. Sci.*, *41*, 846–855.

Hong, G. (2004), Effects of storms on microwave brightness temperatures and its application to estimate cloud parameters using Advanced Microwave Sounding Unit-B, Ph.D. dissertation, Institute of Environmental Physics, University of Bremen, Germany.

Kelley, O., and J. Stout (2004), Convective towers in eyewalls of tropical cyclones observed by the TRMM Precipitation Radar in 1998-2001, paper presented at 20th Conference on Weather Analysis and Forecasting, Amer. Meteor. Soc., Seattle, WA.

Kim, M.-J., G. Skofronick-Jackson, and J. A. Weinman (2003), Intercomparison of millimeter-wave radiative transfer models, paper presented at IEEE International Geoscience and Remote Sensing Symposium (IGARSS), Toulouse, France.

Kummerow, C., W. S. Olson, and L. Giglio (1996), A simplified scheme for obtaining precipitation and vertical hydrometeor profiles from passive microwave sensors, *IEEE Trans. Geosci. Remote Sens.*, *34*, 1213–1232.

Liou, K. N. (1992), *Radiation and cloud processes in atmosphere: Theory, Observation, and Modeling*, 487 pp., Oxford Univ. Press, Oxford.

Liu, G., and J. A. Curry (1999), Tropical ice water amount and its relations to other atmospheric hydrological parameters as inferred from satellite data, *J. Atmos. Sci.*, *38*, 1182–1194.

Luo, Y., S. K. Krueger, G. G. Mace, and K.-M. Xu (2003), Cirrus cloud properties from a cloud-resolving model simulation compared to cloud radar observations, *J. Atmos. Sci.*, *60*, 510–525.

Mace, G. G., E. E. Clothiaux, and T. P. Ackerman (2001), The composite characteristics of cirrus clouds: Bulk properties revealed by one year of continuous cloud radar data, *J. Climate*, *14*, 2185–2203.

Muller, B. M., H. E. Fuelberg, and X. Xiang (1994), Simulations of the effects of water vapor, cloud liquid water, and ice on AMSU moisture channel brightness

temperatures, *J. Appl. Meteorol.*, *33*, 1133–1154.

Peixoto, J. P., and A. H. Oort (1992), *Physics of climate*, 520 pp., American Institute of Physics, New York.

Skofronick-Jackson, G. M., and J. R. Wang (2000), The estimation of hydrometeor profiles from wideband microwave observations, *J. Appl. Meteorol.*, *39*, 1645–1657.

Skofronick-Jackson, G. M., A. J. Gasiewski, and J. R. Wang (2002), Influence of microphysical cloud parameterizations on microwave brightness temperatures, *IEEE Trans. Geosci. Remote Sens.*, *40*, 187–196.

Skofronick-Jackson, G. M., J. R. Wang, G. M. Heymsfield, R. Hood, W. Manning, R. Meneghini, and J. A. Weiman (2003), Combined radiometer-radar microphysical profile estimations with emphasis on high-frequency brightness temperature observations, *J. Appl. Meteorol.*, *42*, 476–487.

Staelin, D. H., and F. W. Chen (2000), Precipitation observations near 54 and 183 GHz using the NOAA-15 satellite, *IEEE Trans. Geosci. Remote Sens.*, *38*, 2322–2332.

Tao, W.-K., and J. Simpson (1993), Goddard cumulus ensemble model. Part I: Model description, *Terr. Atmos. Oceanic Sci.*, *4*, 35–72.

Vivekanandan, J., J. Turk, and V. N. Bringi (1991), Ice water path estimation and characterization using passive microwave radiometry, *J. Appl. Meteorol.*, *30*, 1407–1421.

Wang, J. R., J. Zhan, and P. Racette (1997), Storm-associated microwave radiometric signatures in the frequency range of 90-220 GHz, *J. Atmos. Ocean Technol.*, *14*,

13–31.

Wang, J. R., J. Zhan, and P. Racette (1998), Multiple aircraft microwave observations of storms over the western Pacific Ocean, *Radio Sci.*, *33*, 351–368.

Weng, F., L. Zhao, R. R. Ferraro, G. Poe, X. Li, and N. C. Grody (2003), Advanced microwave sounding unit cloud and precipitation algorithms, *Radio Sci.*, *38*(4), 8068, doi:10.1029/2002RS002679.

Wilheit, T. T., A. T. C. Chang, J. L. King, E. B. Rodgers, R. A. Nieman, B. M. Krupp, A. S. Milman, J. S. Stratigos, and H. Siddalingaiah (1982), Microwave radiometric observations near 19.35, 92 and 183 GHz of precipitation in tropical storm Cora, *J. Appl. Meteorol.*, *21*, 1137–1145.

Zhao, L., and F. Weng (2002), Retrieval of ice cloud parameters using the Advanced Microwave Sounding Unit, *J. Appl. Meteorol.*, *41*, 384–395.

Figure Captions

Figure 1. Cloud types of GCE cloud model data with cloud tops above 8 km at model time 240 min (left) and 360 min (right). The solid black line at $x = 58$ depicts the location of vertical cross section for Figure 2.

Figure 2. Cross sections of liquid water content (cloud liquid water plus rain water), cloud ice water content, snow water content, and graupel water content from the GCE model data at model time 360 min along the line $x = 58$ in Figure 1.

Figure 3. The brightness temperature depressions of the four different cloud types of Figure 1 as a function of surface emissivity.

Figure 4. Jacobians for liquid water water content from the GCE model data at model time 360 min along the line $x = 58$ in Figure 1.

Figure 5. Same as Figure 4 but for cloud ice water content.

Figure 6. Same as Figure 4 but for snow water content.

Figure 7. Same as Figure 4 but for graupel water content.

Figure 8. Jacobians for brightness temperature difference between the 183.3 ± 1 GHz channel and the 183.3 ± 7 GHz channel with respect to hydrometeor water content from the GCE model data at model time 360 min along the line $x = 58$ in Figure 1.

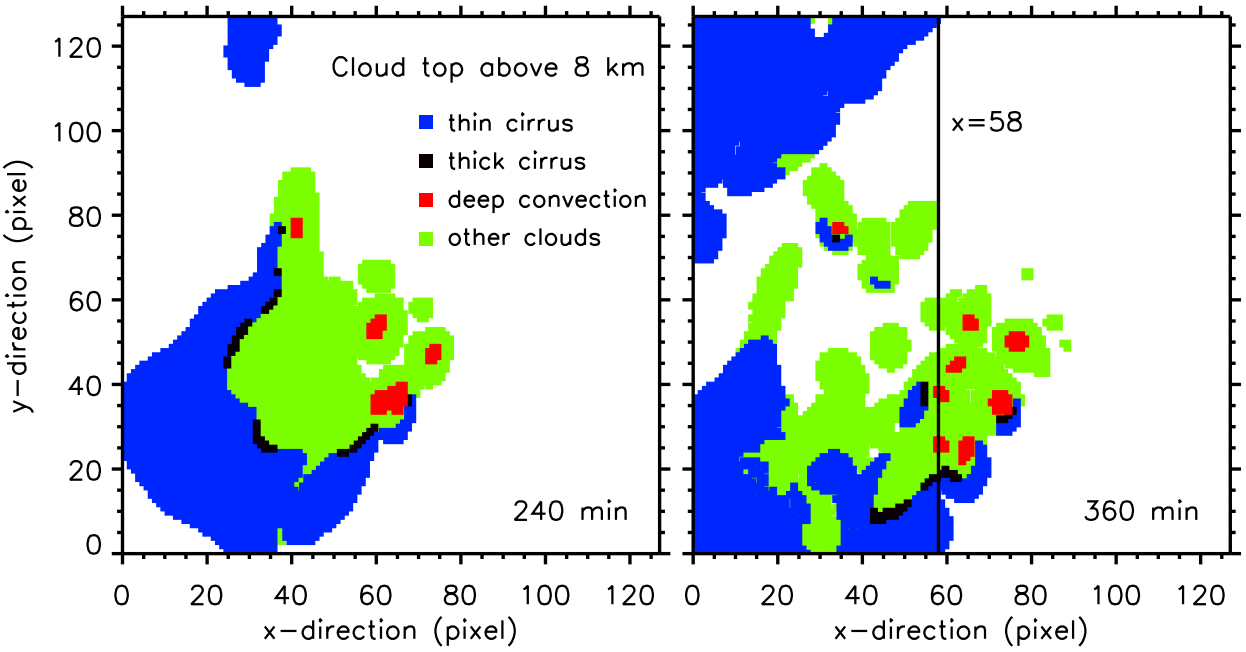

Figure 1. Cloud types of GCE cloud model data with cloud tops above 8 km at model time 240 min (left) and 360 min (right). The solid black line at $x = 58$ depicts the location of vertical cross section for Figure 2.

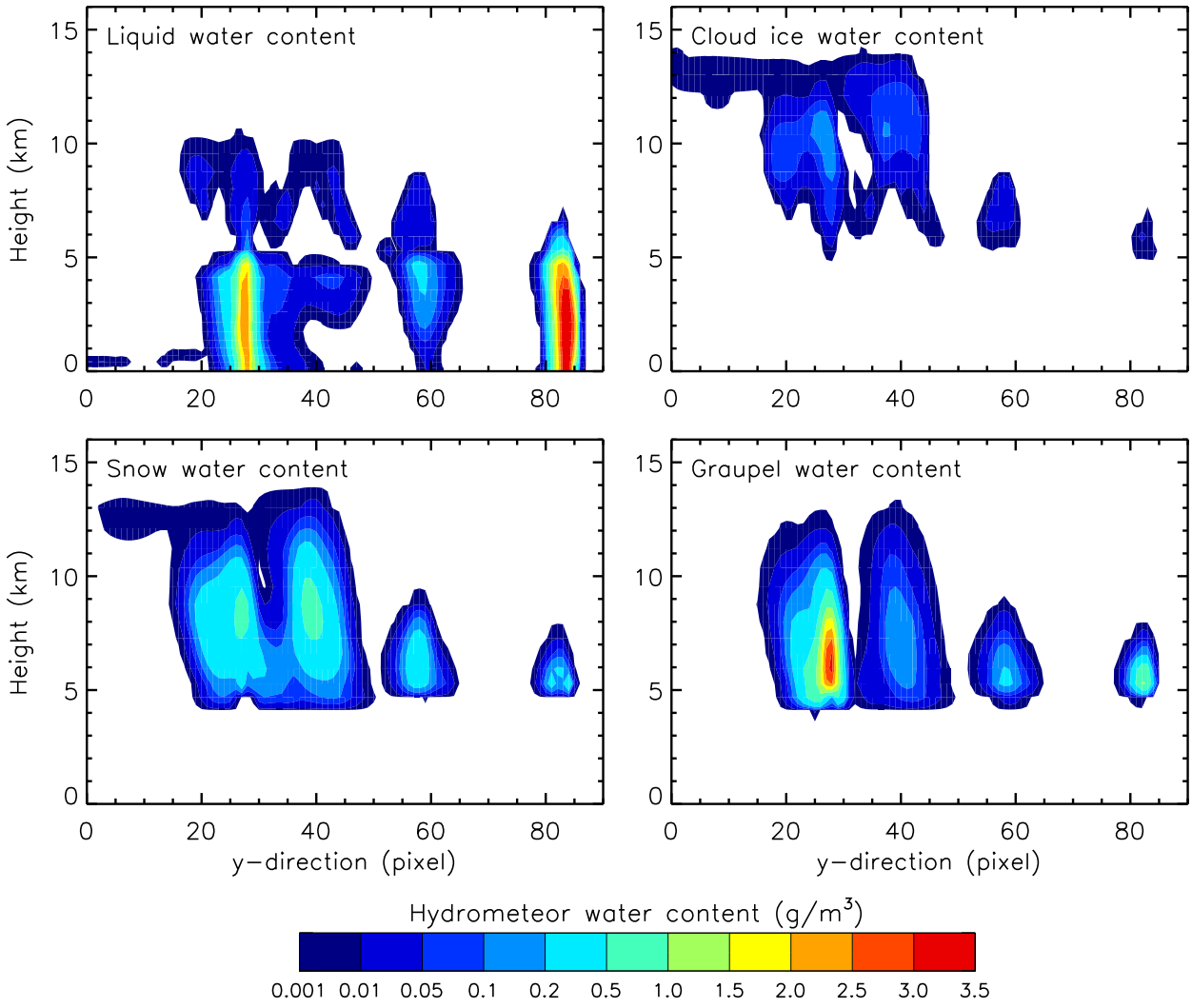

Figure 2. Cross sections of liquid water content (cloud liquid water plus rain water), cloud ice water content, snow water content, and graupel water content from the GCE model data at model time 360 min along the line $x = 58$ in Figure 1.

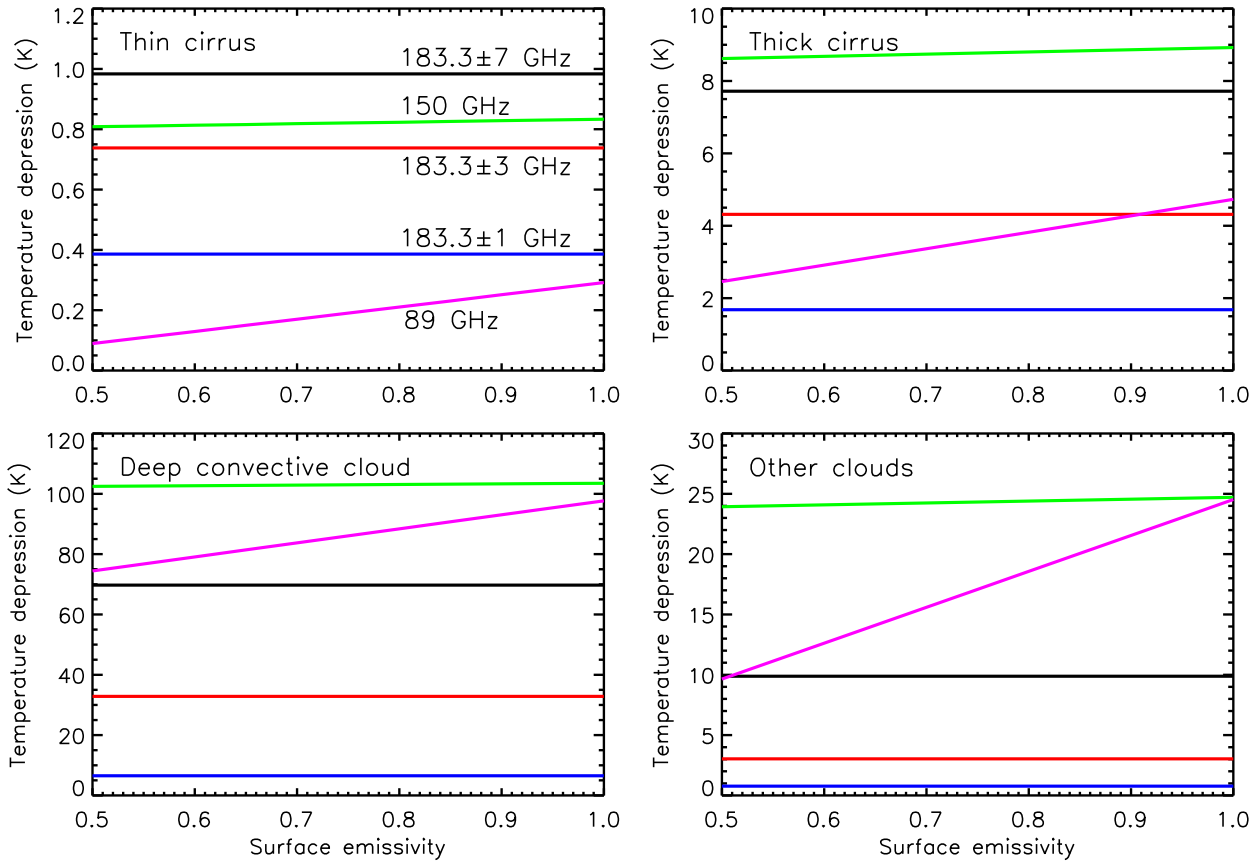

Figure 3. The brightness temperature depressions of the four different cloud types of Figure 1 as a function of surface emissivity.

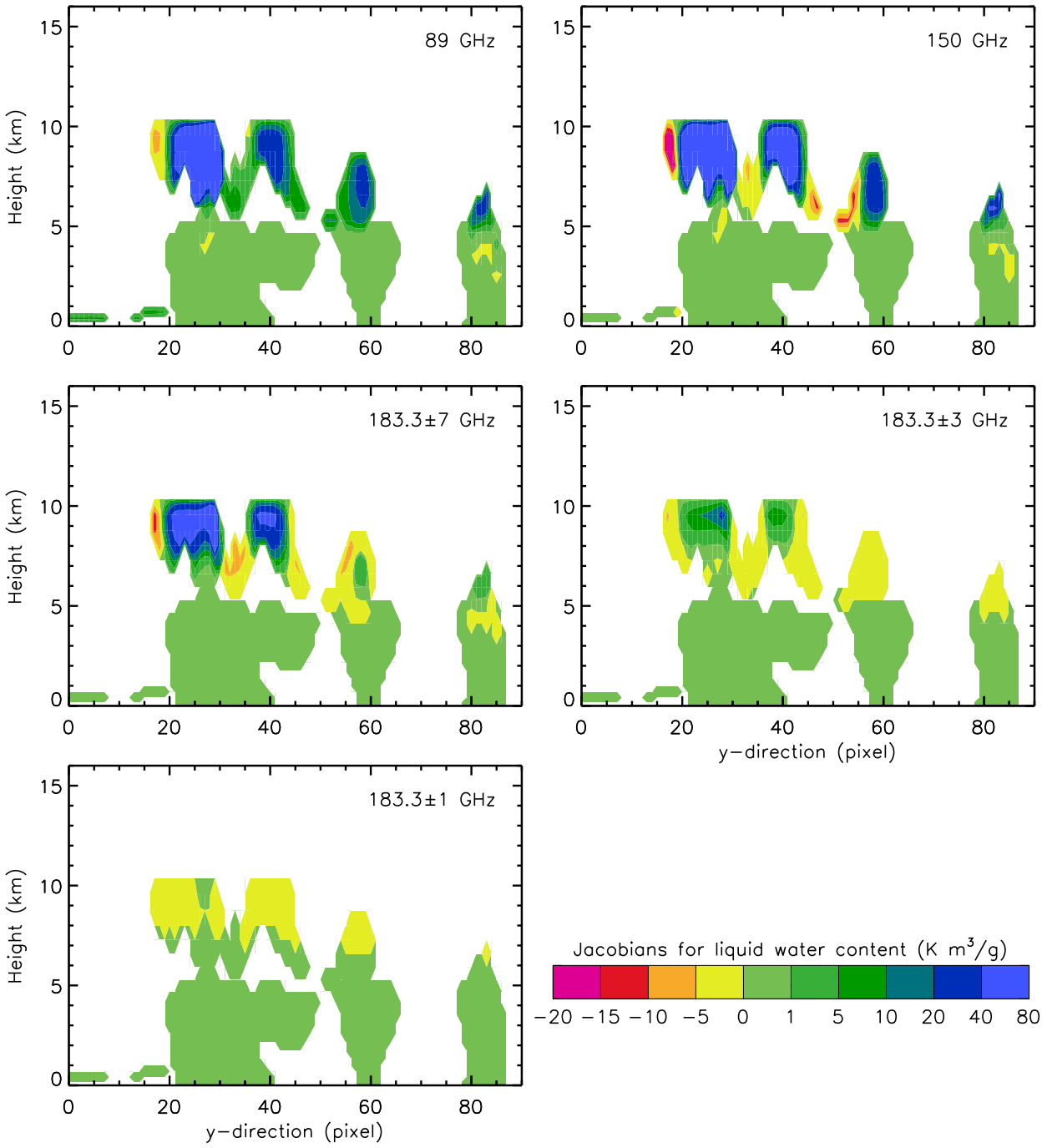

Figure 4. Jacobians for liquid water water content from the GCE model data at model time 360 min along the line $x = 58$ in Figure 1.

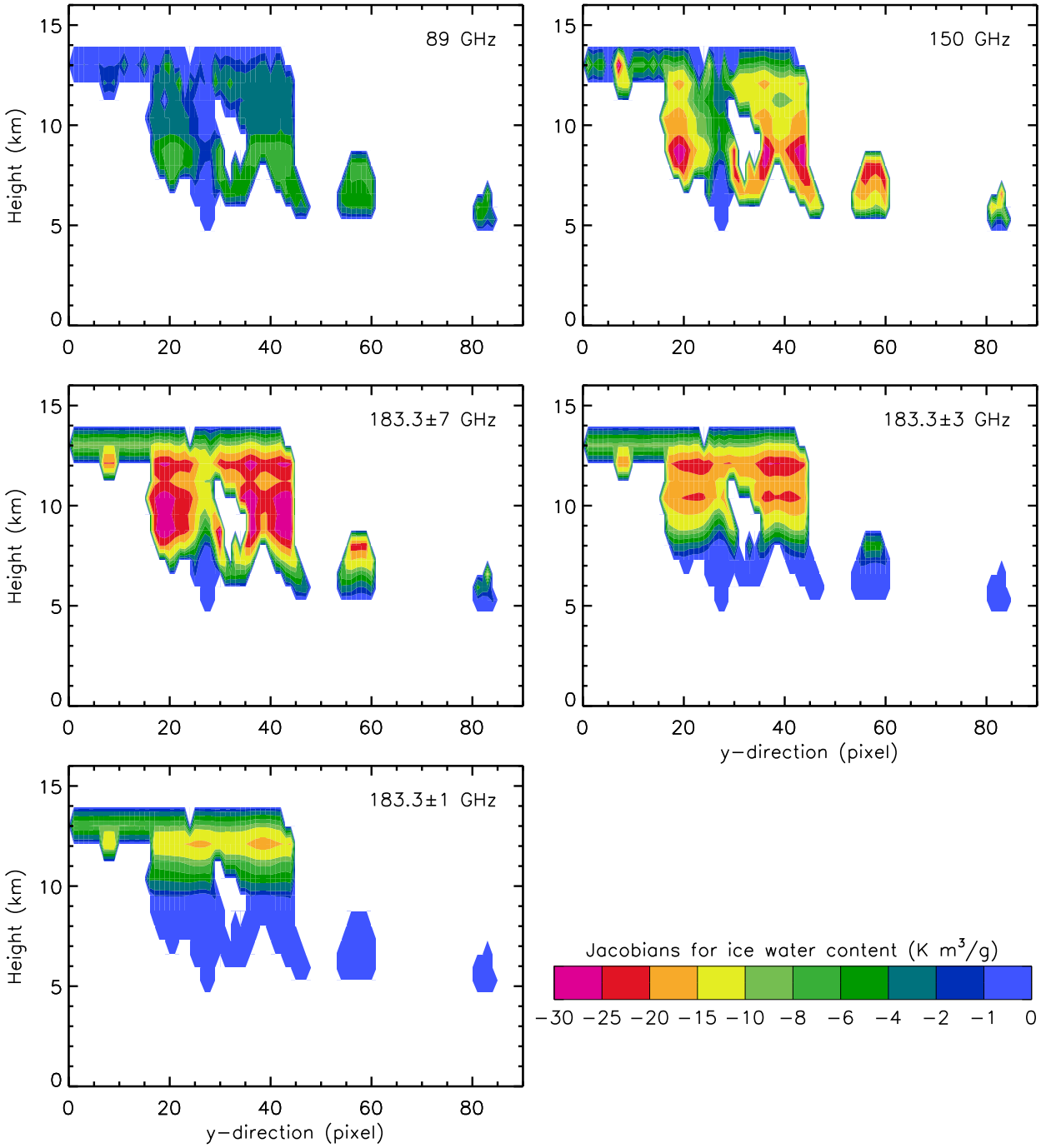

Figure 5. Same as Figure 4 but for cloud ice water content.

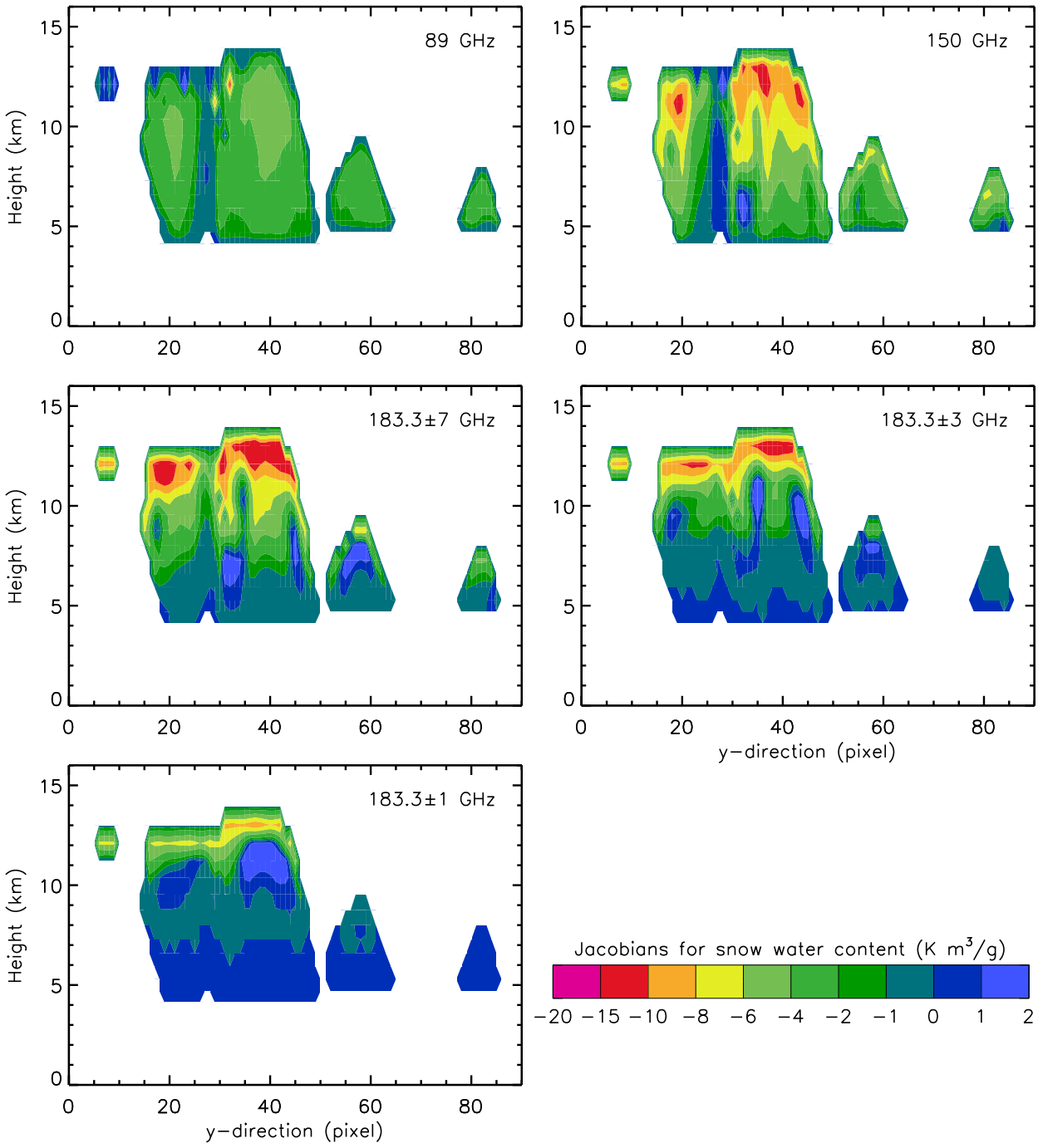

Figure 6. Same as Figure 4 but for snow water content.

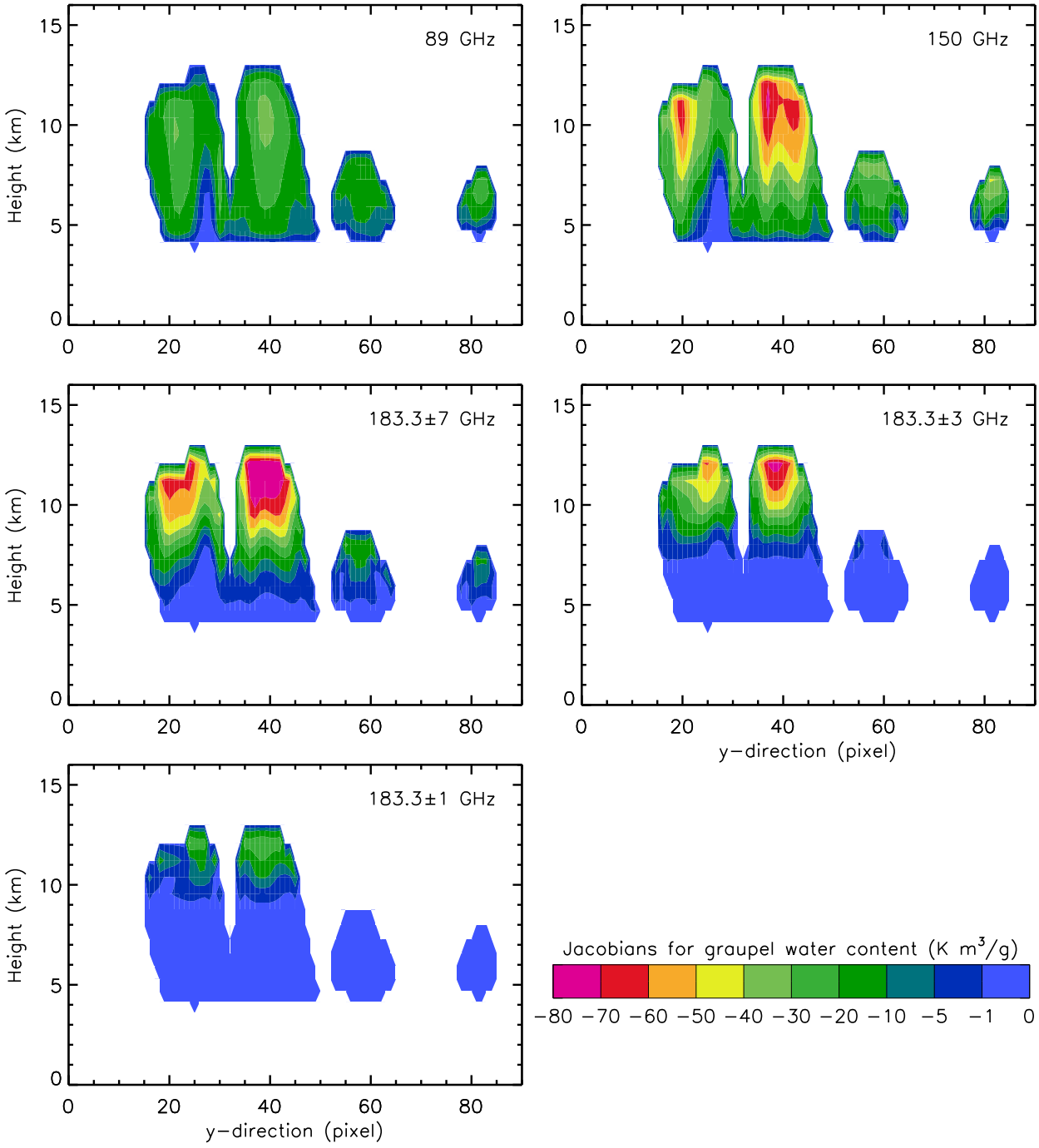

Figure 7. Same as Figure 4 but for graupel water content.

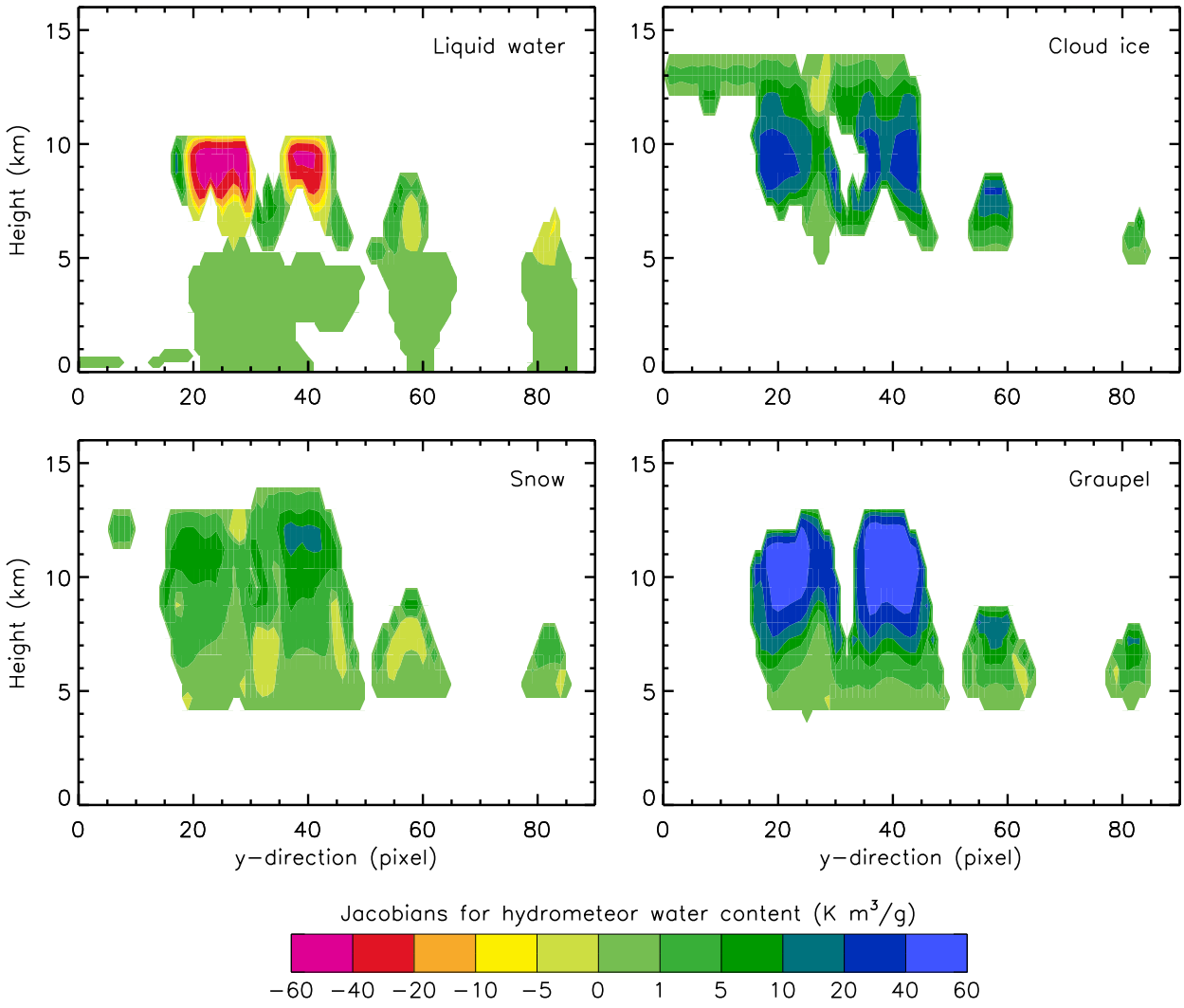

Figure 8. Jacobians for brightness temperature difference between the 183.3 ± 1 GHz channel and the 183.3 ± 7 GHz channel with respect to hydrometeor water content from the GCE model data at model time 360 min along the line $x = 58$ in Figure 1.